FEMS Microbiology Ecology, 95, 2019, fiy219

doi: 10.1093/femsec/fiy219
Advance Access Publication Date: 31 October 2018
Research Article

RESEARCH ARTICLE

Correlation of bio-optical properties with photosynthetic pigment and microorganism distribution in microbial mats from Hamelin Pool, Australia

Amy Fisher[1,2], Daniel Wangpraseurt[3,4,5], Anthony W.D. Larkum[6], Michael Johnson[6], Michael Kühl[3,6], Min Chen[7], Hon Lun Wong[1,2] and Brendan P. Burns[1,2,*]

[1] School of Biotechnology and Biomolecular Sciences, University of New South Wales, Sydney 2052, Australia, [2]Australian Centre for Astrobiology, University of New South Wales, Sydney 2052, Australia, [3]Marine Biological Section, University of Copenhagen, Copenhagen 1017, Denmark, [4]Department of Chemistry, University of Cambridge, Cambridge CB2 1EW, UK, [5]Scripps Institution of Oceanography, University of California, San Diego 92037, CA, USA, [6]Climate Change Cluster, University of Technology, Sydney 2007, Australia and [7]School of Life and Environmental Sciences, University of Sydney, Sydney 2006, Australia

*Corresponding author: School of Biotechnology and Biomolecular Sciences, University of New South Wales, Sydney, 2052, Australia. Tel: +612 93853659; Fax: +612 93851591; E-mail: brendan.burns@unsw.edu.au

One sentence summary: The authors describe for the first time the optical properties and light-harvesting potential of the evolutionarily significant Shark Bay microbial mats

Editor: Ian C Anderson

ABSTRACT

Microbial mats and stromatolites are widespread in Hamelin Pool, Shark Bay, however the phototrophic capacity of these systems is unknown. This study has determined the optical properties and light-harvesting potential of these mats with light microsensors. These characteristics were linked via a combination of 16S rDNA sequencing, pigment analyses and hyperspectral imaging. Local scalar irradiance was elevated over the incident downwelling irradiance by 1.5-fold, suggesting light trapping and strong scattering by the mats. Visible light (400–700 nm) penetrated to a depth of 2 mm, whereas near-infrared light (700–800 nm) penetrated to at least 6 mm. Chlorophyll *a* and bacteriochlorophyll *a* (Bchl *a*) were found to be the dominant photosynthetic pigments present, with BChl *a* peaking at the subsurface (2–4 mm). Detailed 16S rDNA analyses revealed the presence of putative Chl *f*-containing *Halomicronema* sp. and photosynthetic members primarily decreased from the mat surface down to a depth of 6 mm. Data indicated high abundances of some pigments and phototrophic organisms in deeper layers of the mats (6–16 mm). It is proposed that the photosynthetic bacteria present in this system undergo unique adaptations to lower light conditions below the mat surface, and that phototrophic metabolisms are major contributors to ecosystem function.

Received: 23 July 2018; **Accepted:** 30 October 2018

Keywords: Hamelin Pool; stromatolite; microbial mats; phototrophy; chlorophyll; pigments

INTRODUCTION

Microbial mats are dense multilayered communities of microorganisms that colonise a variety of surfaces in the environment (Franks and Stolz 2009). Microbial mats have been found to thrive under extreme conditions of pH, temperature and high salinity characteristics, such as the geothermal springs of Yellowstone National Park, alkaline sulfidic springs, cold Antarctic lakes, and of particular relevance to the current study, the hypersaline environment of Hamelin Pool, Shark Bay, Australia (Vopel and Hawes 2006; Leuko *et al.* 2007; Allen *et al.* 2009; Franks and Stolz 2009; Abed *et al.* 2014; Wong *et al.* 2015; Wong, Ahmed-Cox and Burns 2016). The microbial mats of Shark Bay have been proposed as potentially good analogues to ancient stromatolites, and the persistence of stromatolites in the early Earth rock record suggests they played a major role in the progression of life (Allen *et al.* 2009; Pagès *et al.* 2015). Additionally, photosynthetic activity that occurred in these early systems is thought to have significantly contributed to the oxygenation of the atmosphere (Allen *et al.* 2009).

The physicochemical microenvironment influences the microbial composition and function of microbial mats (Franks and Stolz 2009), and this includes temperature, pH, wave action, salinity and light availability. Recent work in Hamelin Pool by Pagès and colleagues reported that O_2, sulfides, iron (II), phosphates and pH fluctuated strongly over diel cycles in the microbial mats, and this trend was suggested to be due to increased activity of phototrophic members during daytime (Pagès *et al.* 2014, 2015). In addition,, metagenomic analyses have indicated the Hamelin Pool mat systems possess distinct community structures compared to their counterparts in the Bahamas (Ruvindy *et al.* 2016), suggesting a unique mat environment in Shark Bay.

Recent community analyses of Hamelin Pool microbial mats employing rRNA gene sequencing suggest surface-associated phototrophs are able to use oxygenic, anoxygenic and photoheterotrophic light-harvesting pathways (Wong *et al.* 2015). Interestingly, some cyanobacteria increased in abundance with depth in these mats, which has been suggested to be linked to the availability of near-infrared (IR) radiation (i.e. 700–800 nm; NIR) in deeper layers (Wong *et al.* 2015). Some cyanobacteria, such as *Acaryochloris marina*, as well as the recently classified *Halomicronema hongdechloris* from Hamelin Pool stromatolites, can use NIR for photosynthesis (Chen and Blankenship 2011; Chen *et al.* 2010; Chen *et al.* 2012). It has been demonstrated that functional groups of microorganisms organise themselves spatially within a mat (Harris *et al.* 2013; Wong *et al.* 2015), and it has been speculated that such microenvironmental stratification is the result of well-defined optical niches within the mat. Direct measurements of *in vivo* scalar irradiance (i.e. the total quantum flux in a point incident from all directions) would allow for quantifying the spectral light environment available for photosynthesis within different mat layers. To date there is also no information on pigment distribution with depth in Hamelin Pool mats, and determining the pigment composition would confirm the light-harvesting potential of these systems. The aim of the present study was thus to characterise light and phototrophic characteristics at a micrometre scale in the microbial mats of Hamelin Pool, in order to understand the microenvironmental drivers affecting ecosystem function. This was achieved by measuring light penetration through the mat surface, linking with mat pigment composition, and characterising phototrophic community profiles.

MATERIALS AND METHODS

Site description, sampling and mat sectioning. Sampling was undertaken at Nilemah, on the southern shore of Hamelin Pool (26å27'336"S, 114å05.762"E), at 1200h on 21 June 2015. At the time of sampling, the water temperature was 20.1°C, salinity 67.4 PSU (Practical Salinity Units), and pH 8.13. Mat types analysed here were designated smooth mats, as they are extensively distributed in Shark Bay, and have been examined in detail at the taxonomic and metagenomic levels (Wong *et al.* 2015; Ruvindy *et al.* 2016; Wong *et al.* 2017, 2018). A map showing the location of sampling is shown in Fig. 1A. Duplicate mat samples were taken using a sterile scalpel and placed in sterile containers. These mat samples are considered representative of the expansive sheets of these mat types that are found at this location in Shark Bay, as shown by previous studies on the same mats using the same methods of replication (e.g. Wong *et al.* 2017, 2018). Samples were immediately preserved in RNALater (Ambion, Life Technologies) for downstream DNA analyses, and stored at -20°C until further processing. Seawater overlying the mats was also taken at the time of sampling and placed in sterile containers. To facilitate mm-scale analysis of pigment and community composition, mat samples were sliced horizontally at 2 mm depths using sterile blades (Fig. 1B). Mats were sliced into eight sections covering a 16 mm depth (layers designated S1–S8). Sectioned mat slices were stored in individual tubes at -20°C for downstream pigment and DNA analysis.

Scalar irradiance microsensor measurements

Measurements of mat optical properties were conducted in the lab post-sampling on replicate samples of those later sectioned, and DNA extractions were performed. Samples were stored at 4°C prior to scalar irradiance measurements. Measurements of scalar irradiance were conducted using fibre optic microsensors with a tip size of ~50–80 μm (Lassen, Ploug and Jorgensen 1992). Microsensors were mounted on a PC-controlled motorised micromanipulator (Pyroscience GmbH, Germany) at a 45° angle relative to the vertically incident light (Wangpraseurt *et al.* 2012). A 4 × 4 cm portion of 2 cm thick smooth mat sample was submerged in water collected from Shark Bay, Western Australia, in a black acrylic chamber. The sample was illuminated with vertically incident light provided by a tungsten halogen lamp (KL 2500, Schott GmbH, Germany) set to an incident downwelling irradiance (400–700 nm) of ~3000 μmol photons m^{-2} s^{-1}, to simulate light levels reached during midday shallow water conditions (Wangpraseurt *et al.* 2014). Scalar irradiance spectra were recorded with the microsensor connected to a PC-controlled fibre optic spectrometer (USB2000+, Ocean Optics, USA). Microsensor profiles were performed with the automatic motor with step sizes ranging from ~50–130 μm. For depths beyond 2 mm it was necessary to loosen the mat structure with a fine needle (~0.5 mm in diameter) enabling smooth penetration of the light microsensor. Spectra were processed as described previously (Wangpraseurt *et al.* 2012). The diffuse attenuation coefficient (K_0 [mm^{-1}]) was analysed as described previously (Brodersen *et al.* 2014).

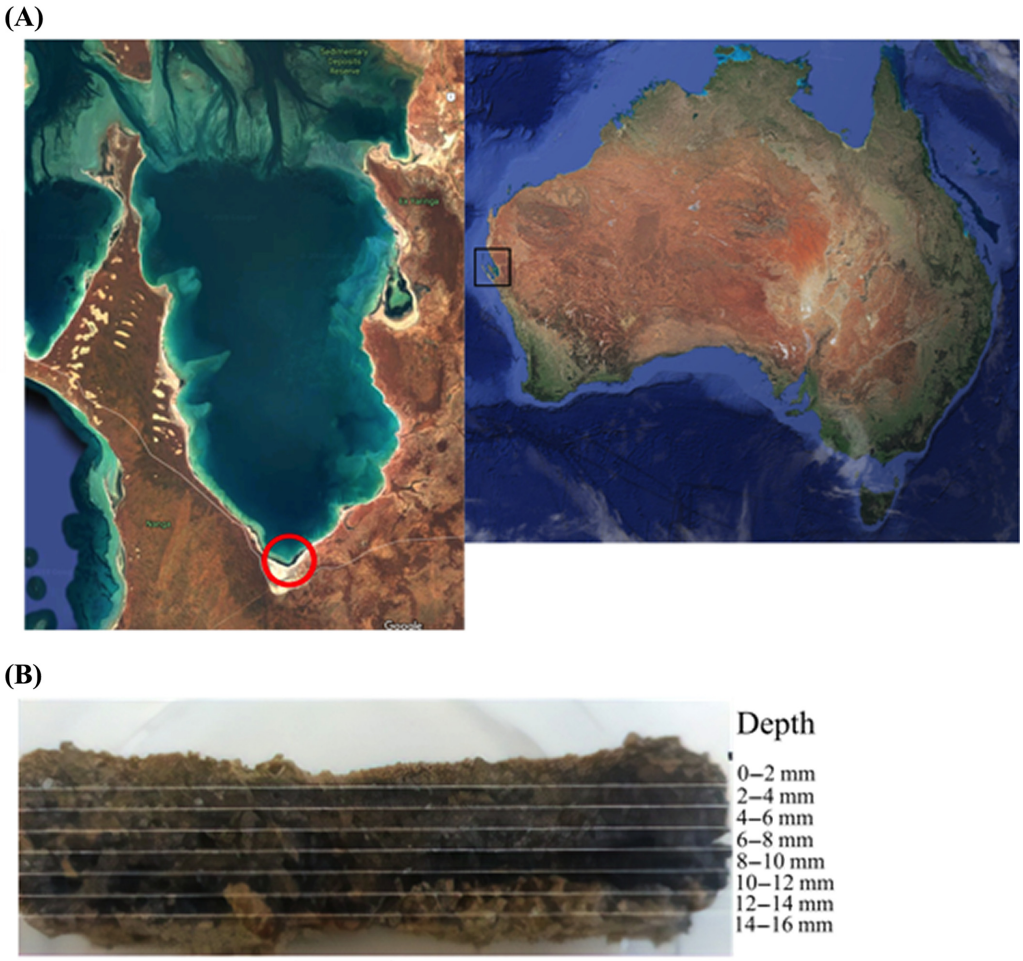

Figure 1. Sample and site location. (**A**) Map showing the relative location of Shark Bay in Australia (black square, right image) and Hamelin Pool (left) in Western Australia. Red circle indicates the site of sampling (Nilemah). (**B**) Vertical cross-section of Shark Bay microbial mats indicating layers analysed in the present study.

Hyperspectral imaging

Hyperspectral imaging was performed in reflectance mode with a hyperspectral camera system (100T-VNIR, Thermvis Vision Systems, St. Louis, MO, USA) mounted via the c-mount on a dissection microscope. Incident illumination was provided by a fibre optic tungsten halogen lamp (see above) connected to a ring light (Trampe and Kühl 2016). Hyperspectral reflectance measurements (%) were performed with a vertical cross-section of the microbial mat (length 2 cm, width 4 cm and height 2 cm) placed in a petri dish (covered with black tape to reduce background reflections) and submerged in a small amount of Hamelin Pool seawater. To measure diffuse spectral reflectance, each hyperspectral scan on the mat was calibrated against a dark current stack (i.e. with the light source switched off; 0% reflectance)) and a 20% light diffusing reference standard (Spectralon, SRM-20; LabSPhere Inc., North Sutton, NH, USA). Hyperspectral cubes were recorded with dedicated imaging software (PhiLumina Hyperspectral Imager V. 4.2: Philumina, LLC, Gulfport, MS, USA). Data analysis was then performed via a combination of custom written codes in Matlab as well as the image processing toolbox (Look@Mosi, Polerecky *et al.* 2009).

Pigment extraction and high performance liquid chromatography (HPLC

All extractions were conducted on duplicate mat layers, in low light conditions to reduce light-induced oxidation of pigment molecules. Water was removed from samples via pre-extraction with 1 mL 100% methanol (meOH) for 30 min before centrifugation and discard of supernatant. Pigments were then extracted from approximately 1 cm^2 (0.3–0.8 g) of each smooth and pustular mat sample using 1 mL of fresh 100% meOH at -20°C overnight. Supernatant extracts were then concentrated to ~200 μL using a vacuum centrifuge for ~15 min. Pigment samples were eluted on a Shimadzu VP HPLC system with a 4.6 mm x 15 cm C_{12} column. Pigments were detected using a Shimadzu SPD-M10A diode array detector with a detection range of 370–800 nm. The program for each sample was 35 min long with a mobile phase flow rate of 1 mL/min. Line A contained 85% meOH with 0.15 M ammonium acetate (NH_4Ac) and line C contained 100% meOH; 100–0% line A with 0–100% line C ran at 0–5 min, 100% line C ran at 5–30 min for elution, then 100–0% line C with 0–100% line A ran at 30–35 min. Pigments were identified based on their spectral absorbance comparability to known pigment data (Scheer *et al.* 2006) at the VPL Biological Pigments database (NASA Astrobiology Institute) and LipidBank (JCBL). Standards are given in Supplementary Table 1. Approximate pigment absorbance ratios

Table 1. Pigment quantities in Shark Bay microbial mats relative to Chl *a* in the same layer as determined by HPLC.

Depth	Scy	β-car	Chl *a*	Phe *a*	Bchl *a*	Unknown
Surface–2 mm	0.00	0.07	1.00	0.02	0.00	0.15
2–4 mm	0.00	0.03	1.00	0.02	1.19	0.24
4–6 mm	0.43	0.50	1.00	0.02	1.03	0.30
6–8 mm	0.33	0.13	1.00	0.02	1.04	0.00
8–10 mm	0.54	0.84	1.00	0.05	0.63	0.00
10–12 mm	0.26	0.79	1.00	0.06	0.32	0.00
12–14 mm	0.32	0.19	1.00	0.03	1.02	0.15
14–16 mm	0.80	0.12	1.00	0.00	0.81	0.37

were calculated as relative ratios to Chl *a* (mono-vinyl chlorophyll a) in the same sample (Table 1). Chl *a* was used as the quasi-standard and approximate pigment quantities were calculated as relative ratios to Chl *a* in the same sample (Table 1). Ratios derived were of the intensity of absorbance (units mAU) of each pigment relative to the mAU of Chl *a*.

Nucleic acid extraction, 16S SSU amplicon sequencing and analysis

Total community DNA was extracted in duplicate from each microbial mat layer employing the MoBio PowerBiofilm DNA Isolation Kit (MO BIO Laboratories, Carlsbad, USA) according to the manufacturer's instructions. Concentrations and purity of extracted DNA were determined spectrometrically, and the quality checked by PCR (Wong *et al.* 2015). Bacterial 16S rRNA genes were paired-end sequenced on an Illumina MiSeq desktop sequencer. Amplicon production was performed using barcoded 27F/519R primers that targeted the V1 to V3 region of the bacterial 16S rRNA gene as previously described (Wong *et al.* 2015).

Sequence data was processed using MOTHUR version 1.33.3 to align and classify bacterial identities into operational taxonomic units (OTUs) as well as to test for sequencing depth and sample diversity. Forward and reverse fastq files were merged together using the 'make.contigs' command in MOTHUR. Sequences were initially screened to remove those longer than 600 bp, containing more than eight homopolymers, and any that contained ambiguous nucleotides. The remaining sequences aligned with the Silva Bacteria Database version 128 (Quast *et al.* 2013). Chimeric sequences were removed in MOTHUR. Sequences were classified taxonomically with the Greengene database (August 2013 release) (DeSantis *et al.* 2006), and subsequently clustered into OTUs at a genetic divergence level of 3%, which represents species level. Following initial screening and alignment to the Silva database, 131 970 sequences were obtained. After removal of high error (more than five nucleotide mismatches) and chimeric sequences, a total of 36 966 sequences remained. The sample with the lowest number of sequences (S8) had 1094 total sequences, hence normalisation to 1090 sequences per sample was used.

OTUs were analysed in Primer 6 version 1.0.1 with the PERMANOVA add on, to group samples based on their taxonomic similarities, then analysed in STAMP version 2.1.3 to identify the significant phylogenetic difference between each group. Finally, correlation networks were created for taxonomic groups using R version 3.2.5 then visualised using Cytoscape version 3.3.0. Rarefaction analysis and non-parametric estimators were performed to determine bacterial diversity and richness using MOTHUR. Similarity matrices using Bray-Curtis similarity were generated using square root-transformed abundance tables. Square root transformation was used to de-emphasize large values and enhance detectability of low-abundance sequences. Principal coordinate (PCO) analyses were generated (including individual replicates from each layer) from the similarity matrices by Primer 6 PERMANOVA to visualise the similarities between mat layers layers. Samples were then clustered based on their similarity and applied as an overlay on the PCO graphs. Bacterial taxa with strong correlation (Pearson's $p > 0.7$) were overlaid on the PCO graph as vectors. Statistical analysis of metagenomic profiles (STAMP) was also undertaken (Parkes *et al.* 2014). Based on Welch's t-test and Benjamini–Hochberg correction, STAMP identifies the taxonomic groups that significantly (corrected *p*-values: $q < 0.05$) contribute to differences in community structure between different depths. Correlation networks between microbial taxa were generated using R studio with the *Hmisc* and *Igraph* library package. Only strong correlations were shown (Pearson's $p > 0.6$, $p < 0.001$). The network was then visualised using Cytoscape.

Data depositing

Sequences have been deposited in Metagenomic Rapid Annotations using Subsystems Technology (MG-RAST) under the project *Phototrophy in Shark Bay microbial mats* and accession numbers 4 798 578.3 to 4 798 678.3 (URL link: https://www.mg-rast.org/linkin.cgi?project = mgp85862).

RESULTS

Optical properties of Hamelin Pool mats

For measurements of mat optical properties, replicate biological samples were analysed and representative data is shown. Diffuse surface reflectance of the mat averaged between 25–50% for visible light (400–700 nm) (Fig. 2a). Reflectivity was lowest between 400–450 nm (˜25–30% reflectivity) and highest between 650–800 nm with reflectance values reaching up to 50% (Fig. 2a). Scalar irradiance microsensors measured that E_0 (scalar irradiance) at the mat surface was enhanced over downwelling irradiance (E_d) with values reaching ˜1.5 times of E_d. A characteristic subsurface enhancement of E_0 was measured for far red to NIR wavelength regions within the first 130 μm of the mat, showing E_0 enhancements of up to 2-fold relative to E_d (Fig. 2b). Shorter wavelengths of visible light (400–500 nm) generally attenuated more rapidly compared with longer wavelengths and most of the 420 nm radiation was attenuated within the first 600 μm of the mat ($E_0 < 0.1\%$ E_d, Fig. 2c).

Light attenuation was highest within 0.5–1 mm of the mat surface (Fig. 3a) and beyond such depths light attenuation continuously decreased. The spectral attenuation coefficient peaked at between 480–510 nm with values of $K_0(\lambda) = 3.5$ (mm^{-1})

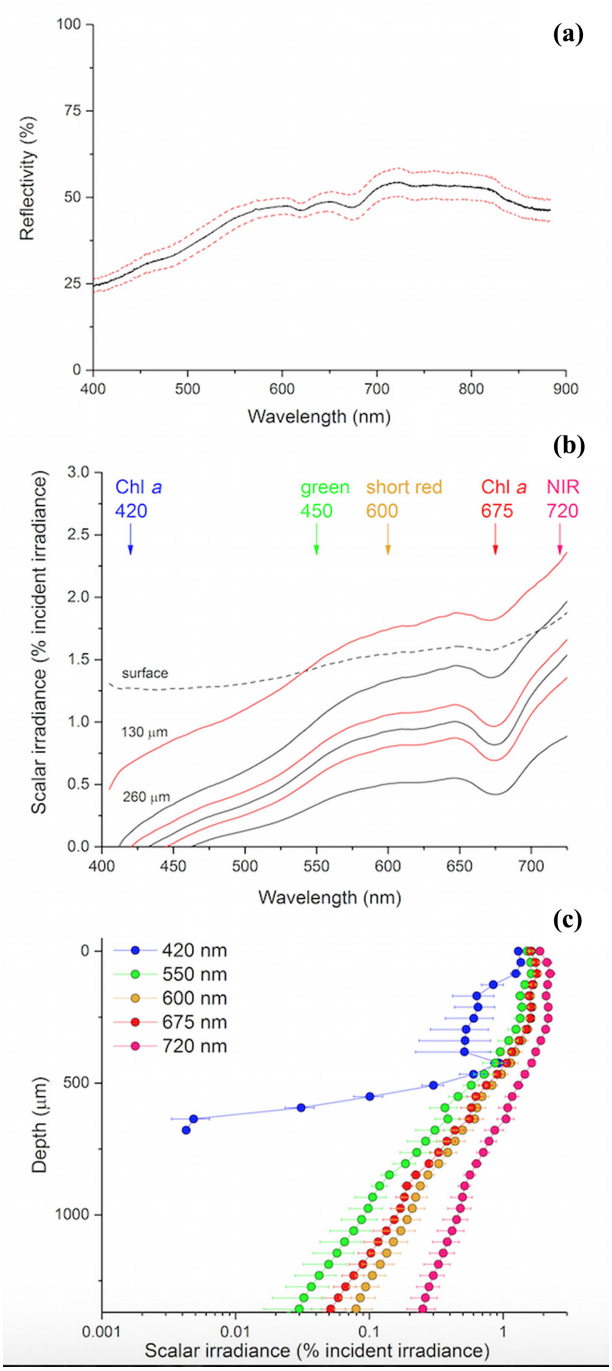

Figure 2. Optical properties of the top layers (< 2mm) of Shark Bay smooth mats. (**a**) Diffuse reflectance (n = 12, data are means ± CI). (**b**) Representative microprofiles of spectral scalar irradiance (normalised to the incident downwelling spectral irradiance, E_d). The dotted black line represents measurements taken at the mat surface and subsequent spectra correspond to increments of 130 μm (see METHODS AND MATERIALS). Spectra are coloured in an alternating fashion (black–red) for clarity. (**c**) Wavelength-dependent penetration of scalar irradiance. Spectral scalar irradiance was averaged for selected wavelengths of interest, indicated by arrows in (b). Data are means ± SE (n = 6).

for a measurement depth of 0.5–1 mm. Signatures of Chl *a* absorption within the first 2 mm of the mat were identified as indicated by shoulders between 670–680 nm (Fig. 3a). Photosynthetically active radiation (PAR) attenuated to ~0.1% of E_d within less than 1.5 mm of the mat surface (Fig. 3b). In contrast, NIR attenuation was much less pronounced, and even at measurement depths of ~5 mm from the mat surface NIR values were ~0.1% of E_d (Fig. 3b).

Pigment distribution

Pigments extracted from Shark Bay mats had a variety of different pigments in all eight layers (Fig. 4). Chlorophyll (Chl) *a* and bacteriochlorophyll (Bchl) *a* were the dominant photosynthetic pigments. β-carotene was present in low levels in all layers. Scytonemin was detected in several layers, and small amounts of pheophytin (Phe) *a* were also detected. A variety of other carotenoids were detected with this method, however, due to the high similarity in their elution times and absorption spectra, were indistinguishable from one another. Some degradation of pigments was evident in all samples in the form of background peaks at irregular elution times. These peaks resembled known spectra of Chl *a*, Phe *a*, and some carotenoids (Fig. 4; pigments 4, 6, 7, 9, 10 and 11).

Chromatograms indicated that the surface layer (0–2 mm) was unique compared to all other layers based on differences in its carotenoid profile and the absence of Bchl *a*, which was present in all preceeding layers (2–16 mm). Based on pigment absorbance ratios (Table 1), Chl *a* was the most abundant photosynthetic pigment in layers 1 (0–2 mm), 5–6 (8–12 mm) and 8 (14–16 mm), whereas the other four layers had slightly more BChl *a*. Scytonemin (Scy) was present in layers 3–8 (2–16 mm). An unknown pigment—potentially BPhe *a*—was present in layers 1–3 (0–6 mm) and 7–8 (12–16 mm). β-carotene (β-car) was present in all layers, and Phe *a* was present in layers 1–7 (0–14 mm). Additionally, hyperspectral imaging of vertical cross-sections of the mat samples revealed spectral signatures distinct for Chl *a* absorption (675 nm) throughout the entire imaged sections and beyond 5 mm of vertical depth (Fig. 5a-d).

Microbial composition and distribution with mat depth

16S rDNA extracted from Shark Bay microbial mats was sequenced using the Illumina MiSeq platform. Rarefaction analysis indicated that curves start to level off but did not yet reach asymptote, indicating further sampling is required to reach saturation of richness. These analyses indicate the surface layer had the lowest diversity with 269 random OTUs per 1000 sequences, while layers S4 (6–8 mm) and S8 (14–16 mm) had the highest at > 500 OTUs per 1000 sequences. Shannon index measurements revealed very high evenness of abundance between species in all samples (Supplementary Table 2). Sample S6 (10–12 mm) showed the highest evenness at 5.84.

With a focus on photosynthetic members, the distribution of taxonomic groups in the Hamelin Pool mats was determined. Based on principal coordinate (PCO) analyses, Cyanobacteria, Proteobacteria and Chloroflexi were highly associated with the top two layers (0–4 mm; Fig. 6). Although Bacteroidetes is not commonly known as being phototrophic, its association with the light-abundant surface of smooth mats was significant. This was evident in both PCO and statistical analysis of metagenomic profiles (STAMP) analyses (Supplementary Fig. 1). Microbial mat layers were grouped by their phylogenetic similarities using Bray-Curtis resemblance (Fig. 6). Group A included the top

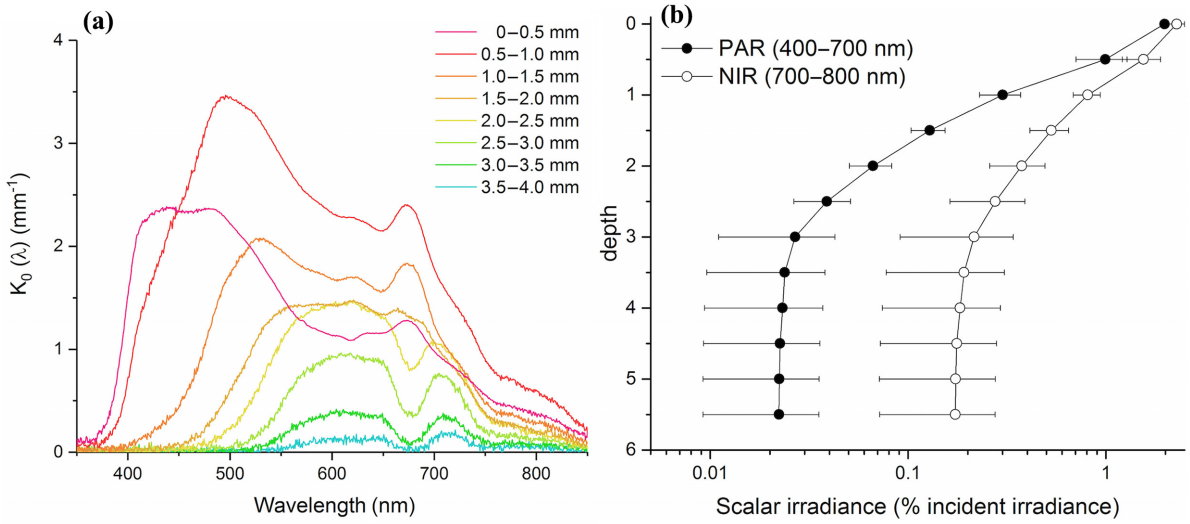

Figure 3. Light attenuation within the photic zone (< 5 mm) of the stromatolite. (**a**) Spectral attenuation coefficient of scalar irradiance $K_0(\lambda)$. (Data are means ± SE, n = 4). Error bars are omitted for clarity. (**b**) Mean photosynthetically available radiation (PAR, 400–700 nm; closed symbols) and near-infrared radiation (NIR, 700–800 nm; open symbols) scalar irradiance profiles. Depth is in mm. Scalar irradiance was normalised to the incident downwelling irradiance. (Data are means ± SE, n = 5).

two layers (surface–4 mm), group B included layers 2–4 (2–8 mm), group C included layers 4–7 (6–14 mm) and group D included layer 8 (14–16 mm). STAMP identified the taxonomic groups that were significantly enriched in community structure based on Welch's t-test and Benjamini–Hochberg correction. The following bacterial taxa, Bacteroidetes (Saprospirales), Chloroflexi (Chloroflexales) and Planctomycetes (Phycisphaerales) were significantly over-represented in the surface layers (group A) when compared to all other layers (Supplementary Fig. 1).

Several non-photosynthetic groups were under-represented at the surface layers, such as Anaerolineae (class) from Chloroflexi (phylum) and Planctomycetes, in which the latter taxon was highly enriched at lower layers (Group C) (Supplementary Fig. 2). Non-photosynthetic Plantomycetes were over-represented in the bottom layer (group D). Correlation networks based on 16S rDNA sequences showed evidence of strong photoaerobic associations (Fig. 7). Cyanobacteria were positively correlated to some Proteobacteria, Chloroflexi (class) and Bacteroidetes members. Anaerolineae (class) were negatively correlated to Chloroflexi, Synechoccophycideae (Cyanobacteria), Saprospirae (Bacteroidetes) and Rhodobacterales (Alphaproteobacteria).

Abundance of photosynthetic taxa with mat depth

The abundances of photosynthetic groups at different depths in the Hamelin Pool microbial mats were compared with other groups (both photosynthetic and non-photosynthetic). Alphaproteobacteria was the overall most dominant photosynthetic group in this ecosystem. In addition, Cyanobacteria, Alphaproteobacteria and Gammaproteobacteria generally showed decreases by depth, with some fluctuations between layers 5–7 (8–14 mm). The two Chloroflexi classes showed contrasting abundances, with Anaerolineae increasing by depth, whereas Chloroflexi (class) was mostly restricted to layers 1–2 (0–4 mm) (Fig. 8).

DISCUSSION

Recent studies on Hamelin Pool microbial mats have characterised in detail bacterial, archaeal and viral communities (Wong *et al.* 2015, 2017; White *et al.* 2018). In the present study, the optical properties, pigment distribution and phylogenetic composition of Hamelin Pool microbial mats were delineated for the first time. Light microsensor probes were used to observe the light penetration through the surface of smooth mats and HPLC was used to observe the pigment composition at different depths. This data was then linked to community structure using well-established 16S rDNA sequencing techniques to facilitate a holistic understanding of phototrophy in these systems.

Optical properties of the Hamelin Pool, Shark Bay mats

Data in the present study describing the properties of the mats in relation to light scattering/wavelength has significantly enhanced our understanding of the type of light availability throughout the Hamelin Pool mats, and how this could be reflected in ecosystem function. Recent findings in Hamelin Pool mats have indicated that oxygen is present in the top 3 mm of the smooth mats analysed in the present investigation (Wong *et al.* 2015), and the present study demonstrated that most of the visible light is attenuated beyond 1.5 mm (Fig. 3b). It is thus evident that oxygenic photosynthesis is confined to the top 1.5–3 mm of the mat. If chlorophyll (Chl) *d*- and *f*-producing Cyanobacteria were present, they would have been detected at ~2–5 mm. While 16S rDNA sequences for *Halomicronema hongdechloris* and unclassified *Halomicronema* species were detected in this mat sample, no red-shifted chlorophylls could be identified by HPLC. However, confocal imaging with spectral detection has revealed cyanobacteria containing both Chl *a* and smaller quantities of Chl *f* at depths between 4.0–6.0 mm (Johnston and Larkum, in preparation). It is also evident that longer wavelengths of light (i.e. beyond 690 nm) can penetrate to at least 6 mm of the mat material (Fig. 2). These lower mat layers are therefore expected to be suited to anoxygenic phototrophs such as Proteobacteria and Chloroflexi (Chen and Blankenship 2011; Cardona 2014). As expected, Proteobacteria were abundant in the top three layers

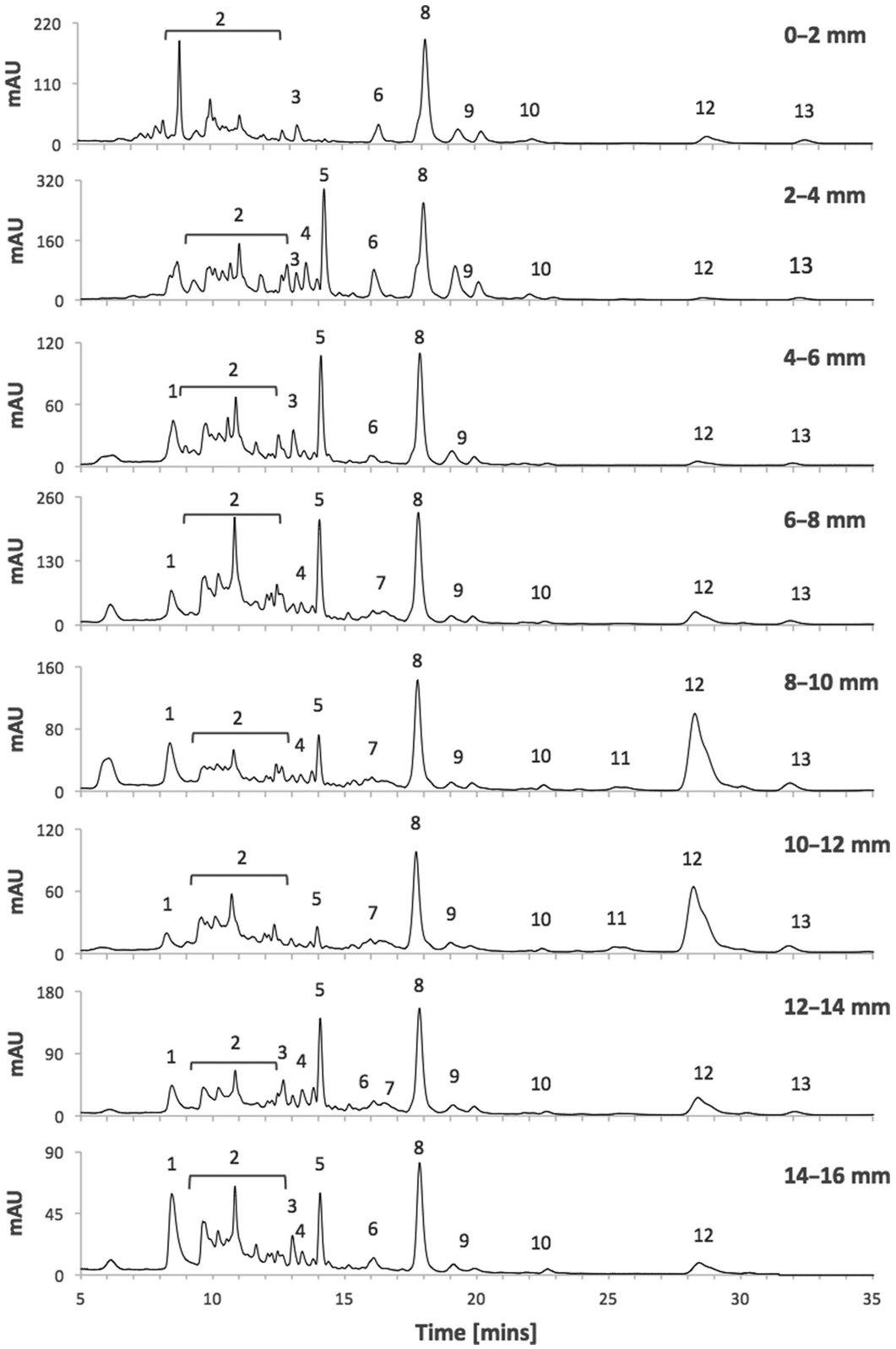

Figure 4. Representative HPLC chromatograms of Shark Bay smooth mat pigments at different sample depths. Peaks represent eluted pigments: Scytonemin (1), carotenoids mixture (2), unknown (3), Chl *a*-like (4), Bchl *a* (5), Chl *a*-like (6), carotenoid-like (7), Chl *a* (8), Phe *a*-like (9), unknown (10), carotenoid-like (11), *β*-carotene (12), Phe *a* (13). Each sample extract was eluted using 100% methanol at a flow rate of 1 mL per min over 35 min. Chl: chlorophyll; Bchl: bacteriochlorophyll; Phe: pheophytin.

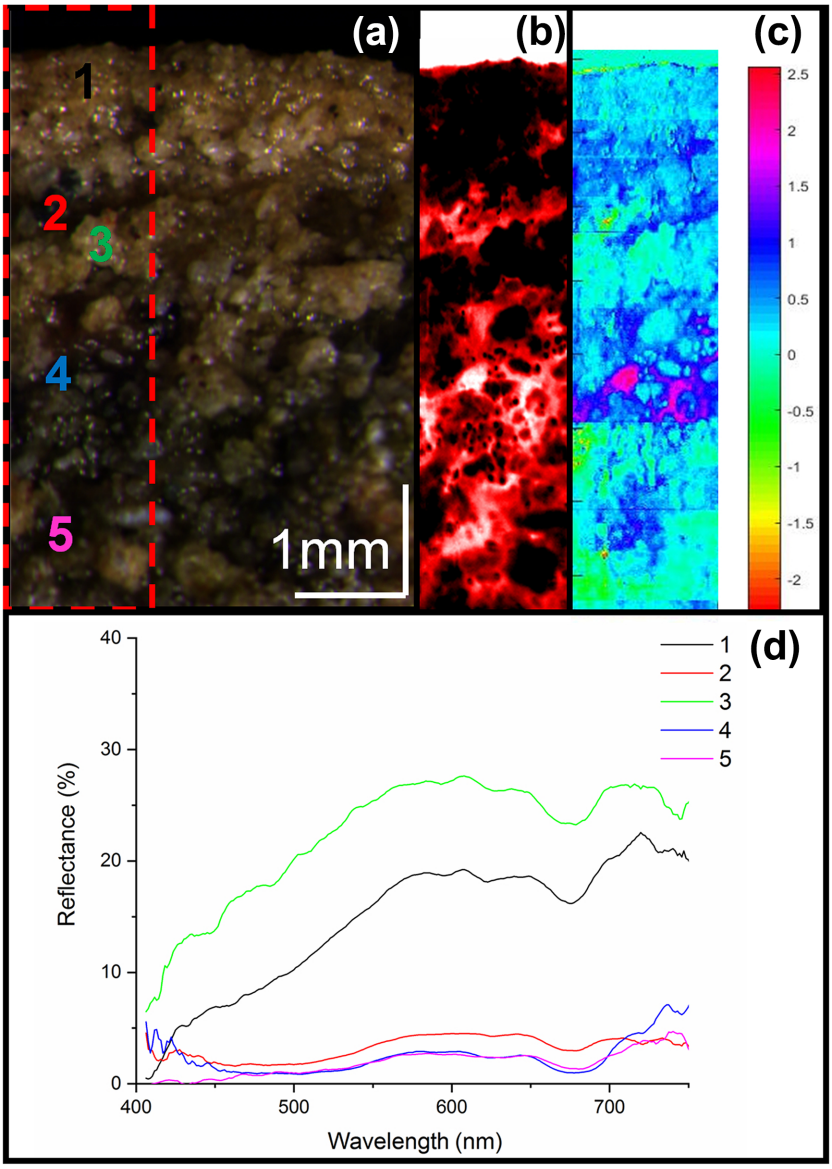

Figure 5. Hyperspectral imaging of Shark Bay microbial mats. (**a**) Combined RGB image from the hyperspectral image stack, using the red channel (650 nm), green channel (550 nm) and blue channel (450 nm) to create true colours. (**b**) False colour-coded hyperspectral image of the image stack shown in the red dotted rectangle in (a), where bright colours (red-white: zmax = 0, black: zmin = -10) indicate chlorophyll *a* absorption based on the log of the fourth derivative of the chlorophyll *a* band (675 nm ± 2 nm). (**c**) False colour-coded chlorophyll *a* absorption based on NDVI (Normalised Difference Vegetation Index) analyses indicating log(R750/675 nm) of the same image stack as in (b). (**d**) Reflectance spectra of the areas marked in (a).

of the smooth mat (surface–6 mm) (Fig. 8). However, their fluctuations at layers 5–7 (8–14 mm) suggest that either IR light is available below 6 mm, or that they are capable of other metabolisms. Indeed, some Proteobacteria members are capable of multiple metabolisms, depending on the environmental conditions (Willey, Sherwood and Woolverton 2008). Chloroflexi members are similarly versatile, with some members showing chemoheterotrophic growth in the dark.

The strong subsurface enhancement of scalar irradiance observed in the top 2 mm of the mat (Fig. 2b) suggests strong scattering and/or light trapping within the mat. The upper layers of these mats are often characterised by the presence of exopolymeric substances (EPS) (Braissant *et al.* 2008) and light trapping by EPS has been reported previously (Decho *et al.* 2003). Such light-trapping phenomena are due to refractive index mismatches between the EPS and the surrounding medium, which causes light scattered from deeper mat layers to be backscattered and thus trapped by the EPS. Such photon-trapping effects would partly explain the high availability of NIR observed in deeper mat layers (Fig. 3b, Decho *et al.* 2003). EPS are typically comprised of polysaccharides and proteins along with other organic and inorganic materials (Cyr and Morton 2006; Braissant *et al.* 2008). Their presence in microbial mats provide a physically and chemically complex matrix which provides structure, as well as facilitates important biological processes such as nutrient transfer and binding of metal ions (Cyr and Morton 2006; Braissant *et al.* 2007, 2008). It has been reported that EPS production in Bahaman stromatolites was highest at the surface layers during daylight hours, suggesting that it is a light-driven process in that system (Decho, Visscher and Reid 2005; Paul *et al.* 2016). It is hypothesised that EPS could therefore be purposefully produced by photosynthetic microorganisms in the Hamelin Pool

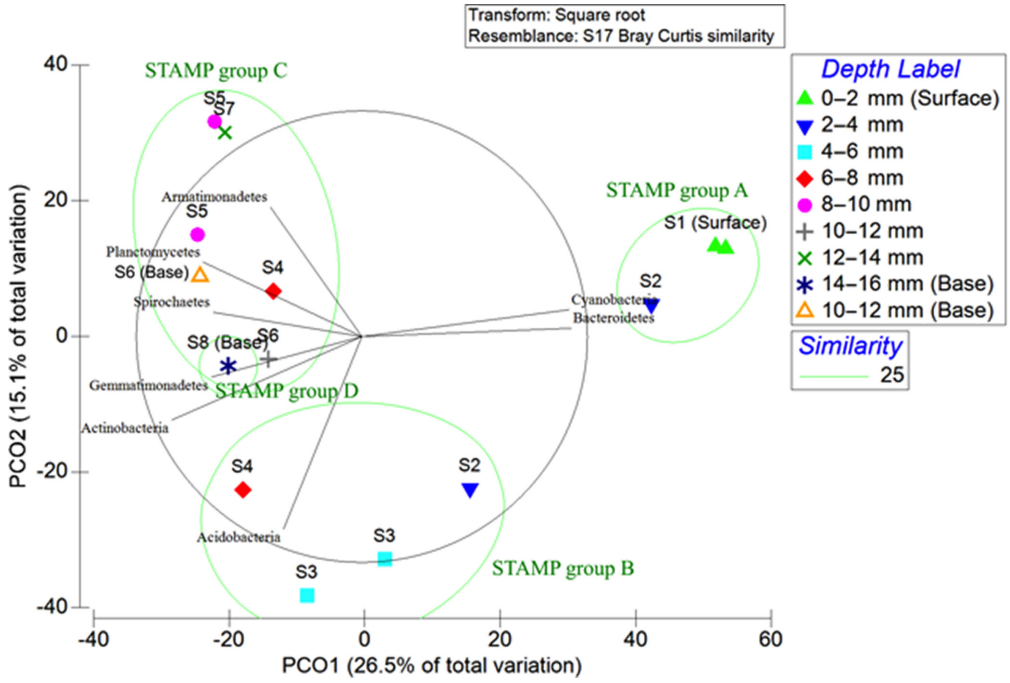

Figure 6. Multilayer principal coordinate analysis of Shark Bay mats with phylogenetic and similarity cluster overlay. Symbols represent individual samples and are clustered based on Bray-Curtis similarity. Solid green circles show samples with 25% or more similarity and are approximately separated by depth. The photosynthetic phylum Cyanobacteria, along with the non-photosynthetic Bacteroidetes are highly associated with the surface layers. Proteobacteria is associated with the second layer (2–4 mm). Duplicates of each layer were used in these analyses.

mats, to enhance light availability in the photic regions and provide a potential evolutionary selective advantage for these systems.

Pigments and light availability in Hamelin Pool mats

Evaluation of pigment distribution with depth in Hamelin Pool microbial mats has highlighted the diverse nature of these systems in terms of light utilisation. Primary light harvesting machinery is produced by photosynthetic bacteria in the presence of light, and production of antenna complexes is inhibited in high light conditions (Chennu *et al.* 2015; Herbstová *et al.* 2010). The pigments detected in the different layers of Hamelin Pool microbial mats should therefore reflect the availability of light at those depths. However, pigment composition did not show a consistent relationship with the light that was available or with the bacteria present. For example, the abundance of scytonemin at layers below the surface (2–16 mm) was unexpected, since it is an ultraviolet (UV) protective pigment produced by cyanobacteria (Rochera *et al.* 2013), which were notably more abundant at the surface. Indeed, past pigment analyses on polar microbial mats have observed high abundances of scytonemin at the surface layers, which decreased by depth (Lionard *et al.* 2012; Rochera *et al.* 2013). In addition, while the high bacteriochlorophyll (Bchl) *a* in layers 2–4 (2–8 mm) reflects the availability of IR light at those depths, Chl *a* was more abundant than Bchl *a* in layers 5–6 (8–12 mm) and 8 (14–16 mm), although visible red light was attenuated at the surface layer (surface–2 mm). It is well known that cyanobacteria will migrate vertically through microbial mat systems to access optimal light conditions for photosynthesis as well as to avoid strong UV exposure (Chennu *et al.* 2015), and this could potentially be occurring in the Hamelin Pool mats.

The results from the present study are consistent with findings from a microbial mat from a hypersaline lake (Lake Chiprana, Spain) that showed similar irregularities in pigment results and suggested that it was likely due to varying sulfide levels (Bachar *et al.* 2008). Sulfide is a substrate used by *Chloroflexaceae* for photoautotrophic growth, and is also a strong reducing agent of BChls *a* and *c* (Bachar *et al.* 2008). Its presence in the Hamelin Pool mat samples could therefore have prevented complete extraction and detection of active bacteriochlorophylls, as well as influenced the abundance of Chloroflexi in certain layers.

In addition, a diverse carotenoid composition was also maintained throughout the mat. Pigmented heterotrophic bacteria produce many types of pigments such as carotenoids, phenazines, melanins, quinones, violacein and flexirubins. For many of these organisms, their pigments are secondary metabolites which can facilitate photoprotection, predation, defence from predation, metal tolerance, oxidation defence or heat tolerance (Kim 2013). It is therefore unlikely that all carotenoids detected in this mat ecosystem are instrumental to phototrophic metabolisms.

Photosynthesis and heterotrophy

Analysis of microbial community composition via 16S rDNA analyses facilitated the correlation (both positive and negative) of Hamelin Pool microbial mat members. Network correlation of 16S rDNA sequences showed links between phototrophic and heterotrophic bacteria (Fig. 7), and strong negative correlations between aerobic and anaerobic members. The two negatively correlated Chloroflexi (phylum) are of interest: Chloroflexi (class) were mostly confined to the top two layers (surface–4 mm). Chloroflexi (class) have members that are capable of both anoxygenic photosynthesis and oxygen respiration (Klatt *et al.* 2011). Such

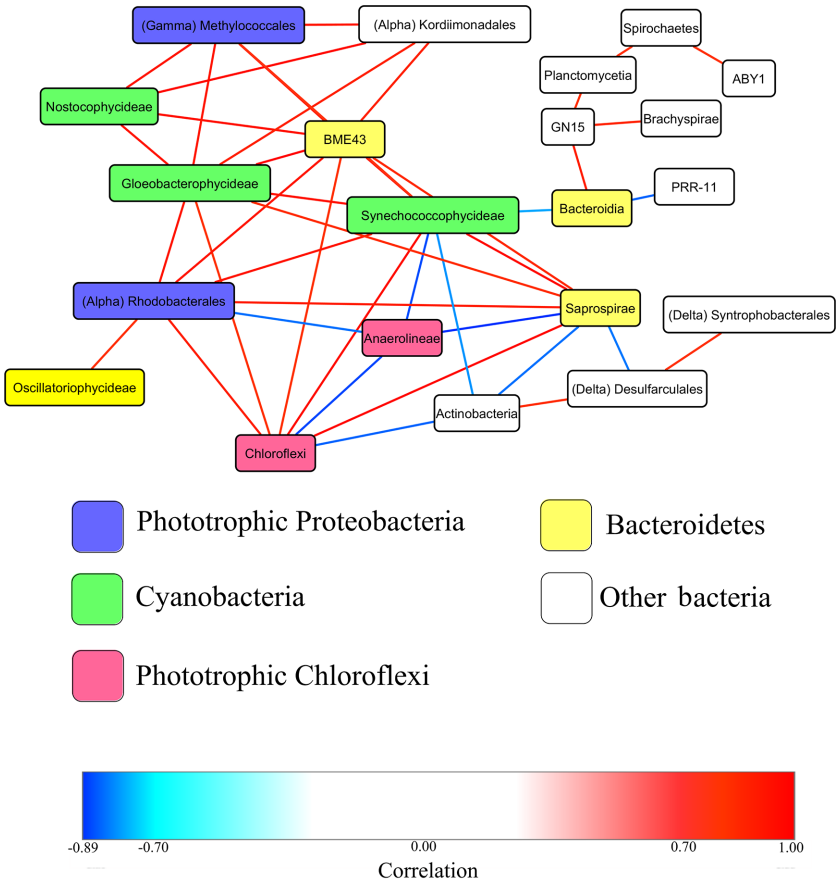

Figure 7. Photoaerobic network of Shark Bay mats community members based on Pearson correlation. Groups with correlation values higher than 0.7 or lower than -0.7 are shown. Red lines indicate positive correlation above 0.7, blue lines indicate negative correlation below -0.7. Node colours indicate phyla of interest to this study, node labels indicate class. Proteobacteria are further separated by order, indicated by node labels with class in parentheses.

members are thus likely to favour the upper layers of this microbial mat environment. In contrast, Anaerolineae were notably less abundant in the top two layers than subsequent layers (Fig. 5). While some members of Anaerolineae have recently been identified as being anoxygenic phototrophs, this class of bacteria more commonly consists of anaerobic heterotrophs (Klatt *et al.* 2011; Campbell *et al.* 2014; Kim and Liesack 2015). It is therefore possible that the majority of Anaerolineae members in this ecosystem correspond to the latter.

As previously observed, Bacteroidetes were one of the major groups that were positively correlated to phototrophic members in Hamelin Pool mats (Wong *et al.* 2015). Classified Bacteroidetes have been shown to have fermentative, as well as anaerobic and aerobic chemoheterotrophic metabolisms, with different members being able to digest cellulose, chitin, pectin or agar (Willey, Sherwood and Woolverton 2008). Some groups also produce orange to yellow pigments such as carotenoids and flexirubins independent of light (Kim 2013). Research on high-temperature chlorophototrophic mats showed undescribed Bacteroidetes members were not chlorophototrophs themselves, rather they had genes for use in fermentation and degradation of complex carbon molecules (Klatt *et al.* 2013). It is therefore possible that the Bacteroidetes members in Hamelin Pool microbial mats occupy the upper layers to utilise the large molecules generated by the highly productive phototrophic bacteria. On the other hand, the localisation of Bacteroidetes at the surface of a different hypersaline microbial mat system was thought to suggest phototrophic capacity (Schneider *et al.* 2013). In addition, halotolerant Bacteroidetes were found at the surface of an inverted salt flat microbial mat, where they showed an inverse relationship with the salt-intolerant cyanobacteria at the bottom (McKay *et al.* 2016). Since it is still uncertain whether Bacteroidetes are capable of phototrophy or other light-induced processes, further investigation into members from the Hamelin Pool microbial mats could provide useful insight into this diverse taxonomic group.

Distribution of phototrophic bacteria with mat depth

Principal coordinate (PCO) analyses showed that photosynthetic groups at the phylum level were generally associated with the top two layers (0–4 mm). Cyanobacteria—oxygenic photoautotrophs—were mostly associated with the top layer (surface–2 mm) while the metabolically diverse Chlorolexi and Proteobacteria showed more even association with all layers (Fig. 6). In addition, the inverse distributions of Chloroflexi and Anaerolineae reflected the network correlation findings (Fig. 7). Although Chl *f* could not be detected via HPLC in the present study, 16S rDNA sequences most closely related to *Halomicronema* sp.—including the Chl *f* producer *Halomicronema hongdechloris*—were detected at depths below 3 mm in the mats.

These inconsistencies between the pigment and sequencing data highlight some difficulties with HPLC measurements. Cyanobacteria such as *Halomicronema hongdechloris* have low ratios of Chl *f* versus Chl *a*, and considering they may be present

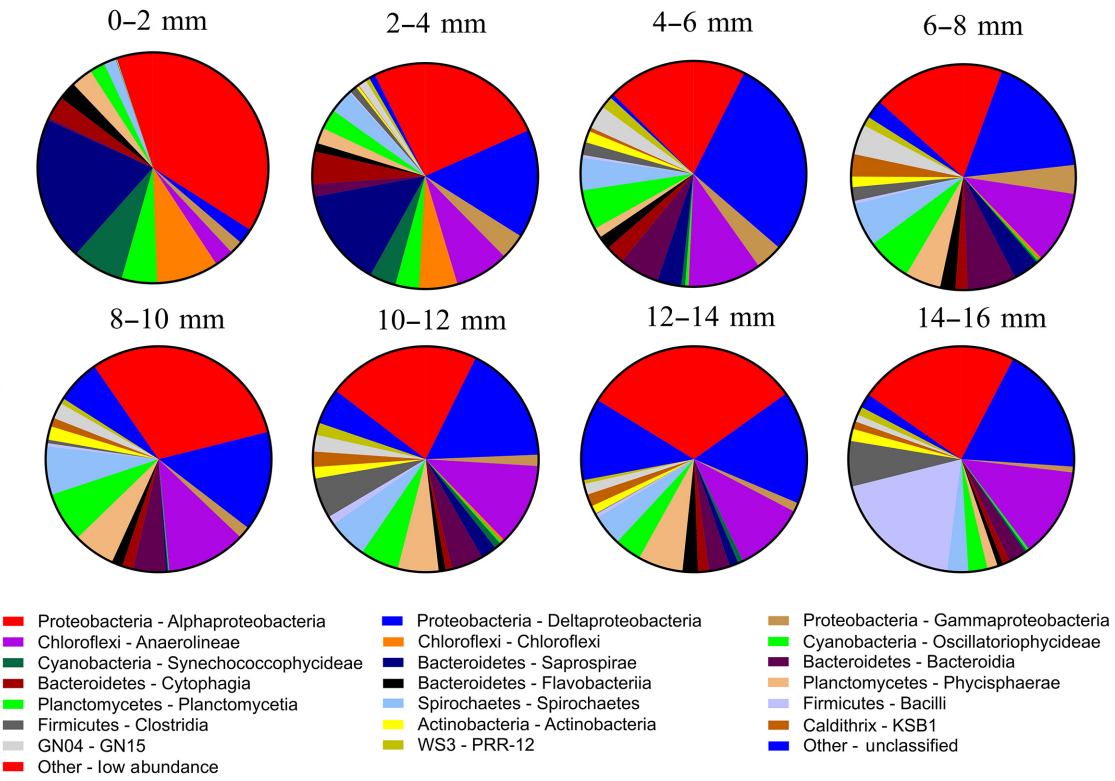

Figure 8. Bacterial distribution in Shark Bay microbial mats at 2 mm depth intervals. Each pie chart shows separate proportions of the 20 overall most abundant classes, and collective proportions of unclassified and low abundance classes. Labels indicate phylum first, followed by class. The average of the duplicates in each layer were used to obtain and plot community composition.

with numerous other cyanobacteria with only Chl *a*, it is not surprising that they are difficult to detect *in situ* in the mats. New photosynthetic members of presumed non-phototrophic groups are frequently found through metagenomics, as well as through the improvement of culturing techniques, as was the case with the recently described phototrophic Acidobacteria and Gemmatimonadetes species (Klatt *et al.* 2011; Cardona 2014). *Gemmatimonas* sp. AP64 is thought to have acquired its photosynthetic genes through a single gene transfer event (Zeng *et al.* 2014). The same study also examined metagenomes of environmental samples and found that other Gemmatimonadetes members could also be phototrophic. Similarly, an uncultured non-photosynthetic member of Cyanobacteria was recently found in symbiosis with a eukaryotic alga (Cardona 2014). As such, metagenomics studies can provide an additional assessment of the phototrophic potential of the organisms in Hamelin Pool microbial mats through the identification of pigment synthesis pathways and reaction centre genes. Indeed, during the course of the present investigation, metagenomic analyses of these mats identified chlorophyll and bacteriochlorophyll synthesis genes in particular, peaking at the surface and subsurface (0–4 mm) (Wong *et al.* 2018).

CONCLUSIONS

This study was the first to delineate light properties, pigment distribution, and link to the phylogenetic and metabolic functioning of Hamelin Pool mats. It was found that a light-trapping effect was present at the top 0.5 mm of the mats, which enhanced light availability in that region. While chlorophyll *a* and bacteriochlorophyll *a* were the dominant photosynthetic pigments in both systems, their distribution in the mat was not consistent with the availability of light at depths below 6 mm. It is therefore possible that high pigment production rates alongside vertical migration in response to varying light intensities is an integral aspect of these mats. This multiphase approach to examine phototrophy has highlighted some important new aspects of the Hamelin Pool mat ecosystems that may be contributing to this important mode of energy production. Further studies into EPS production, pigment composition and confocal imaging for analysis *in situ* of Chl *f* pigments will further improve our understanding of how light is used in Hamelin Pool microbial mats, as well as how light-harvesting metabolisms contribute to overall ecosystem function.

SUPPLEMENTARY DATA

Supplementary data are available at *FEMSEC* online.

FUNDING

This work was supported by a Carlsberg distinguished postdoctoral fellowship to DW.

Conflicts of interest. None declared.

REFERENCES

Abed RMM, Polerecky L, Habsi A *et al.* Rapid recovery of cyanobacterial pigments in desiccated biological soil crusts following addition of water. *PLoS ONE* 2014;**9**: 1–7.

Allen M, Goh F, Burns BP *et al*. Bacterial, archaeal and eukaryotic diversity of smooth and pustular microbial mat communities in the hypersaline lagoon of Shark Bay. *Geobiology* 2009;**7**:82–96.

Bachar A, Polerecky L, Fischer JP *et al*. Two-dimensional mapping of photopigment distribution and activity of Chloroflexus-like bacteria in a hypersaline microbial mat," *FEMS Microbiology Ecology* 2008;**65**:434–48.

Braissant O, Decho A, Dupraz C *et al*. Exopolymeric substances of sulfate-reducing bacteria: Interactions with calcium at alkaline pH and implication for formation of carbonate minerals. *Geobiology* 2007;**5**:401–11.

Braissant O, Decho AW, Przekop KM *et al*. Characteristics and turnover of exopolymeric substances (EPS) in a hypersaline microbial mat. *FEMS Microbiol Ecol* 2008;**67**:293–307.

Brodersen KE, Lichtenberg M, Ralph PJ *et al*. Radiative energy budget reveals high photosynthetic efficiency in symbiont-bearing corals. *J Royal Soc Interface* 2014; 11:20130097.

Campbell AG, Schwientek P, Vishnivetskaya T *et al*. Diversity and genomic insights into the uncultured Chloroflexi from the human microbiota. *Environ Microbiol* 2014;**16**:2635–43.

Cardona T. A fresh look at the evolution and diversification of photochemical reaction centers. *Photosynth Res* 2014;**126**:111–34.

Chen M, Schliep M, Willows RD *et al*. A red-shifted Chlorophyll. *Science*, 2010;**329**:1318–19

Chen M, Blankenship R. Expanding the solar spectrum used by photosynthesis. *Trends Plant Sci* 2011;**16**:427–31.

Chen M, Li Y, Birch D *et al*. A cyanobacterium that contains chlorophyll f – a red-absorbing photopigment. *FEBS Letters*, 2012;**586**:3249–54.

Chennu A, Grinham A, Polerecky L *et al*. Rapid reactivation of cyanobacterial photosynthesis and migration upon rehydration of desiccated marine microbial mats. *Front Microbiol* 2015;**6**:1–9.

Cyr H, Morton KE. Distribution of biofilm exopolymeric substances in littoral sediments of Canadian Shield lakes: the effects of light and substrate. *Can J Fish Aquat Sci* 2006;**63**:1763–76.

Decho AW, Kawaguchi T, Allison MA *et al*. Sediment properties influencing upwelling spectral reflectance signatures: The "biofilm gel effect". *Limnol Ocean* 2003;**48**:431–43

Decho A, Visscher P, Reid R. Production and cycling of natural microbial exopolymers (EPS) within a marine stromatolite. *Palaeogeo Palaeoclim Palaeoecol* 2005;**219**:71–86.

Desantis TZ, Hugenholtz P, Larsen N *et al*. Greengenes, a Chimera-Checked 16S rRNA Gene Database and Workbench Compatible with ARB. *Appl Environ Microbiol* 2006;**72**:5069–72.

Franks J, Stolz J. Flat laminated microbial mat communities," *Earth Sci Rev* 2009;**96**:163–72.

Harris JK, Caporaso JG, Walker JJ *et al*. Phylogenetic stratigraphy in the Guerrero Negro hypersaline microbial mat. *ISME J* 2013;**7**:50–60.

Herbstová M, Litvín R, Gardian Z *et al*. Localization of Pcb antenna complexes in the photosynthetic prokaryote *Prochlorothrix hollandica*. *Biochim et Biophys Acta Bioenerg* 2010;**1797**:89–97.

Kim SK. *Marine biomaterials characterisation, isolation and applications*, Boca Raton: CRC Press, Taylor & Francis Group, 2013.

Kim Y, Liesack W. Differential assemblage of functional units in paddy soil microbiomes. *PLOS ONE*, 2015;**10**:1–20.

Klatt CG, Wood JM, Rusch DB *et al*. Community ecology of hot spring cyanobacterial mats: predominant populations and their functional potential. *ISME J* 2011;**5**:1262–78.

Klatt CG, Inskeep WP, Herrgard MJ *et al*. Community structure and function of high-temperature chlorophototrophic microbial mats inhabiting diverse geothermal environments. *Front Microbiol* 2013;**4**:1–23.

Lassen C, Ploug H, Jorgensen B. A fibre-optic scalar irradiance microsensor: application for spectral light measurements in sediments. *FEMS Microbiol Ecol* 1992;**86**:247–54.

Leuko S, Allen MA, Goh F *et al*. Analysis of intergenic spacer region length polymorphisms to investigate the halophilic archaeal diversity of stromatolites and microbial mat. *Extremophiles* 2007;**11**:203–10.

Lionard M, Péquin B, Lovejoy C *et al*. Benthic cyanobacterial mats in the high Arctic: multi-layer structure and fluorescence responses to osmotic stress. *Front Microbiol* 2012;**3**:1–10.

McKay CP, Rask JC, Detweiler AM *et al*. An unusual inverted saline microbial mat community in an interdune Sabkha in the Rub' al Khali (the Empty Quarter), United Arab Emirates. *PLOS ONE*, 2016;**11**:1–17.

Pagès A, Welsh D, Teasdale P *et al*. Diel fluctuations in solute distributions and biogeochemical cycling in a hypersaline microbial mat from Shark Bay, WA. *Marine Chem* 2014;**167**:102–12.

Pagès A, Grice K, Welsh D *et al*. Lipid biomarker and isotopic study of community distribution and biomarker preservation in a laminated microbial mat from Shark Bay, Western Australia. *Microbial Ecol* 2015;**70**:459–72.

Parkes DH, Tyson GW, Hugenholtz P *et al*. STAMP: Statistical analysis of taxonomic and functional profiles. *Bioinformatics* 2014;**7**:1–2.

Paul VG, Wronkiewicz DJ, Mormile MR *et al*. Mineralogy and microbial diversity of the microbialites in the yypersaline Storr's Lake, the Bahamas. *Astrobiology*, 2016;**16**:282–300.

Polerecky L, Bissett A, Al-Najjar M *et al*. Modular spectral imaging system for discrimination of pigments in cells and microbial communities. *Appl Environ Microbiol* 2009;**75**:758–71

Quast C, Pruesse E, Yilmaz P *et al*. The SILVA ribosomal RNA gene database project: improved data processing and web-based tools. *Nucl Acid Res* 2013;**41**:590–6.

Rochera C, Villaescusa JA, Velázquez D *et al*. Vertical structure of bi-layered microbial mats from Byers Peninsula, Maritime Antarctica. *Antarctic Sci* 2013;**25**:270–6.

Ruvindy R, White RA, Nielan BA *et al*. Unravelling core microbial metabolisms in the hypersaline microbial mats of Shark Bay using high-throughput metagenomics. *ISME J* 2016;**10**:183–96.

Scheer H. An overview of chlorophylls and bacteriochlorophylls: biochemistry, biophysics, functions and applications,"In Grimm B, Porra R, Rudiger W *et al*.(eds), *Chlorophylls and bacteriochlorophylls: biochemistry, biophysics, functions and applications*, Dordrecht: Springer, 2006;1–26.

Schneider D, Arp G, Reimer A *et al*. Phylogenetic analysis of a microbialite-forming microbial mat from a hypersaline lake of the Kiritimati Atoll, Central Pacific. *PLoS ONE*, 2013;**8**:1–14.

Trampe E, Kühl M. Chlorophyll *f* distribution and dynamics in cyanobacterial beachrock biofilms. *J Phycol* 2016;**52**:900–96.

Vopel K, Hawes I., Photosynthetic performance of benthic microbial mats in Lake Hoare, Antarctica. *Limnology and Oceanography*, 2006;**52**:1801–12.

Wangpraseurt D, Larkum AWD, Ralph PJ *et al*. Light gradients and optical microniches in coral tissues. *Front Microbiol* 2012;**3**:1–9.

Wangpraseurt D, Polerecky L, Larkum AW *et al*. The *in situ* light microenvironment of corals. *Limnol Oceanogr* 2014;**59**:917–26.

White RA, Wong HL, Ruvindy R *et al*. Viral communities of Shark Bay modern stromatolites. *Frontiers Microbiol* 2018;**9**:1223. doi: 10.3389/fmicb.2018.01223.

Willey J, Sherwood L, Woolverton C. *Prescott, Harley & Klein's microbiology*, 7th edition, New York: McGraw Hill, 2008.

Wong HL, Smith DL, Visscher PT *et al*. Niche differentiation of bacterial communities at a millimeter scale in Shark Bay microbial mats. *Sci Rep* 2015;**5**:1–17.

Wong HL, Ahmed-Cox A, Burns BP. Molecular ecology of hypersaline microbial mats: current insights and new directions. *Microorganisms* 2016;**4**:E6. doi: 10.3390/microorganisms4010006.

Wong HL, Visscher PT, White RA *et al*. Dynamics of archaea at fine spatial scales in Shark Bay mat microbiomes. *Sci Rep* 2017;**7**: Article No. 46160.

Wong HL, White RA, Visscher PT *et al*. Disentangling the drivers of functional complexity at the metagenomic level in Shark Bay microbial mat microbiomes. *ISME J* 2018;**12**:2619–39.

Zeng Y, Feng F, Medova H *et al*. Functional type 2 photosynthetic reaction centers found in the rare bacterial phylum Gemmatimonadetes. *PNAS USA* 2014;**111**:7795–800.